Corrosion Science 174 (2020) 108855

Contents lists available at ScienceDirect

Corrosion Science

journal homepage: www.elsevier.com/locate/corsci

Abundance of Fe(III) during cultivation affects the microbiologically influenced corrosion (MIC) behaviour of iron reducing bacteria *Shewanella putrefaciens*

Nina Wurzler[a,*], Jan David Schutter[a], Ralph Wagner[b], Matthias Dimper[a], Dirk Lützenkirchen-Hecht[b], Ozlem Ozcan[a]

[a] Bundesanstalt für Materialforschung und -prüfung (BAM), Unter den Eichen 87, 12205, Berlin, Germany
[b] Fakultät für Mathematik und Naturwissenschaften – Physik der kondensierten Materie, Bergische Universität Wuppertal, Gauss Strasse 20, 42097, Wuppertal, Germany

ARTICLE INFO

Keywords:
A. Stainless steel
A. Iron
B. XANES
B. Cyclic voltammetry
C. Microbiological corrosion

ABSTRACT

The effect of the presence of Fe(III) during the cultivation on the electrochemical activity and corrosion behaviour of dissimilatory iron reducing bacteria *Shewanella putrefaciens* was studied by means of ex situ and in situ X-ray absorption near-edge spectroscopy (XANES). Stainless steel AISI 304 and thin iron films were studied as substrates. XANES analysis indicated an accelerated iron dissolution and growth of an oxide/hydroxide film for the culture grown with Fe(III) in comparison to the culture grown in absence of Fe(III). Electrochemical analysis indicated that the biofilm resulted in acceleration of the general corrosion but provides protection against local corrosion.

1. Introduction

Austenitic stainless steels are used in a wide range of applications due to their mechanical properties and corrosion resistance. Under atmospheric conditions, a 1 − 3 nm thin protective passive film is formed on the surface of stainless steels, mainly composed of iron and chromium oxides and hydroxides [1,2]. The chemical composition, structure and electrochemical properties of the passive film determine the corrosion resistance of stainless steels. In solutions of neutral pH the passive films are reported to form a bilayer with an n-type iron oxide/hydroxide-rich outer layer and a p-type chromium oxide/hydroxide-rich inner layer [3–5]. Even though stainless steels are characterized by a high corrosion resistance, microbial activity can still alter the structure and chemistry of the passive film and spatial heterogeneity of the biofilm can promote microbiologically influenced corrosion (MIC) [6–8].

Shewanella species are dissimilatory metal reducing bacteria, which can utilize Fe(III), Mn(IV), Cr(VI) and other inorganic/organic compounds as electron acceptors [9–12]. In the literature, there is no consensus on the role of iron reducing bacteria on the microbiologically influenced corrosion (MIC) of iron and steels [13,14]. On one hand, Fe (III) respiration may lead to the reductive dissolution of the Fe(III) oxy-hydroxide protective layer, enhancing and accelerating the deterioration of the steel [14,15]. On the other hand, recent studies have demonstrated that, under some conditions, iron reducing bacteria can inhibit corrosion processes on steels due to the oxygen scavenging effect of the ferrous ions formed via the reductive dissolution of Fe(III) oxy-hydroxide rich passive films [8,14,16]. Another aspect determining the role of microorganisms in corrosion is the heterogeneity of the biofilm. It is widely accepted that the patchy nature of biofilms can lead to the establishment of local cathodic and anodic regions on the steel surface, which facilitates corrosion processes [16].

In a recent study Miller et al. demonstrated that *Shewanella oneidensis* MR-1 has a protective effect on carbon steel when the biofilm is directly in contact with the metal surface, which is explained with the oxygen dissipating effect of the biofilm by a combination of metabolic consumption and by reaction with biogenic ferrous ions. However, if a second biofilm-free surface is brought to electrical contact with the surface containing the biofilm by means of a zero resistance ammeter (ZRA), the corrosion of the uncovered surface was enhanced by at least a factor of two [8]. These findings have a significant contribution on the understanding of MIC in technical systems, where the biofilm coverage is heterogeneous.

Surface sensitive spectroscopic methods such as X-Ray photoelectron spectroscopy (XPS) applicable for the chemical analysis of the corrosion products formed at a biofilm - metal interfaces require ultra-

* Corresponding author.
E-mail address: nina.wurzler@bam.de (N. Wurzler).

https://doi.org/10.1016/j.corsci.2020.108855
Received 7 February 2020; Received in revised form 25 May 2020; Accepted 3 July 2020
Available online 03 July 2020

high vacuum conditions and the removal of the biofilm. Procedures for removal of the organic films and excessive sample drying under vacuum can also be destructive for the interfacial corrosion products and can cause changes in the chemistry of the corrosion products due to re-oxidation processes [1,17]. To avoid biofilm removal and to minimize the time from coupon extraction out of the incubation until surface analysis, in this study, X-ray absorption near-edge spectroscopy (XANES) was used as the main method for the characterization of the corrosion products.

The application of in situ electrochemical X-Ray Absorption Near-Edge Spectroscopy (XANES) to iron [18–21] and iron/chromium alloys [19] was previously reported as a successful tool for the analysis of passive film chemistry. Schmuki et al. [18] reported a conversion of Fe (III) containing passive films to a porous layer of mainly Fe(II) oxide/hydroxides during reduction processes in alkaline solutions. Furthermore, Davenport and Sansone have reported that anodic polarization of iron at +0.4 V vs. MSE in a pH 8.4 borate buffer solution yields a passive film chemistry composed of a mixture of Fe_2O_3/Fe_3O_4. Virtanen et al. studied electrochemically induced changes on model iron oxide thin films in acidic solutions [22] and observed a strong increase of the iron oxide film dissolution and an oxide film dominated by Fe(II) species. According to Kerkar et al. [19] the passive film on iron can be described as a disordered lepidocrocite (γ-FeOOH) and for FeCr alloy samples or iron samples passivated in chromate containing solutions, chromium is incorporated into the passive layer as a $Cr(OH)_3$-like phase. In a recent study, Wurzler et al. reported an in situ electrochemical XANES investigation of the changes in oxide chemistry on thin iron films in the presence of electrochemically active metal reducing bacteria cultivated with and without the addition of Fe(III) in the cultivation medium [21]. The reported data indicated that cultures pre-exposed to Fe(III) during cultivation have an acceleration of iron dissolution and formation of oxide films containing high amounts of Fe^{2+} species. Monnier et al. analysed the reduction and reoxidation processes of corrosion products formed on iron by means of transmission mode XANES. Their findings indicate that magnetite (Fe_3O_4) and iron (II) hydroxides are formed by the reduction of lepidocrocite and ferrihydrite [17].

Even though the application of XANES to the analysis of corrosion products on various metals [19,22–24] and polymer/metal interfaces [25,26] is well established, it is not widely established for the analysis of MIC related processes. Especially when applied in grazing-incidence geometry, XANES is a powerful tool for gathering information on the changes occurring at environmental interfaces. The application of grazing angle X-ray spectroscopy to environmental interfaces was reviewed by Trainor et al. with the presentation of a model formalism for quantitative analysis of fluorescent yield profiles [27].

The biofilm growth cycle encompasses different stages starting with the initial physical attraction of planktonic bacteria to a substrate, ending with the eventual liberation of cell clusters from the fully grown biofilm matrix due to different reasons such as nutrient limitation [28]. According to our hypothesis, bacteria released from the biofilm on an actively corroding site shall be exposed to a different chemical environment than planktonic bacteria. In this work, as the main parameter, the abundance of ferric ions in the cultivation media of model microorganism *Shewanella putrefaciens* was investigated in terms of its effect on the microbiologically influenced corrosion of AISI 304 grade stainless steel and model iron films. The surface analysis was complemented by electrochemical and microscopic studies to characterize the differences in corrosion behaviour.

2. Experimental

2.1. Substrate preparation

Austenitic stainless steel sheets of type AISI 304 (1.4301) were cut into coupons (15 mm x 15 mm) and ground with silicon carbide abrasive paper up to 600 grit (P1200). The surface was rinsed and cleaned with acetone in an ultrasonic bath for ten minutes. For all experiments, steel coupons were pre-conditioned potentiostatically for one hour at +50 mV vs. open circuit potential (OCP) in a 20 mM $NaClO_4$ electrolyte to assure reproducibility of the surface chemistry. For the investigations on model iron surfaces, 80 nm thick iron films have been deposited via electron-beam evaporation deposition (10^{-8} mbar, 15 W, CreaTec, Erligheim, Germany) on Kapton© (polyimide) foils [21].

Table 1
Composition of Shewanella Minimal Medium (ShMM), adapted from M9 minimal medium, Miller et al., 1972 [29]).

NH_4Cl	15.0 mM
Na_2SO_4	7.0 mM
$MgSO_4$	0.4 mM
$CaCl_2$	0.4 mM
Na glutamate	1.5 mM
KH_2PO_4	4.25 mM
Na_2HPO_4	4.25 mM
Na lactate	8.96 g L^{-1}

2.2. Cultivation of microorganisms

Shewanella putrefaciens CN32 (ATCC-BAA-1097, LGC Standards GmbH, Wesel, Germany) was batch cultivated in Erlenmeyer flasks at 28 °C in a minimal medium with composition as listed in Table 1 (*Shewanella* Minimal Medium (ShMM), adapted from M9 minimal medium, Miller et al., 1972 [29]). To investigate the effect of pre-exposure to Fe(III) during cultivation, two cultures were grown in ShMM with (referred to as FeCi in the text) and without (referred to as CN32 in the text) the addition of Fe(III)-citrate. For the FeCi culture a mixture of 2-fold concentrated ShMM was mixed 50:50 vol% with 16 g/l Fe(III) citrate (Sigma Aldrich, technical grade, adjusted to pH 7) solution. Cultures were grown overnight and washed three times at 1510 rcf for 4 min and re-suspended in sterile ShMM after centrifugation to prepare the incubation media with a final OD_{600} of 0.1 [21]. Additionally, control experiments were performed by extracting the supernatant via filtration of the cultures without any further dilution. Those are referred to as CN32-filtrate and FeCi-filtrate in the following sections.

2.3. XANES measurements

Ex situ X-ray absorption near edge spectroscopy (XANES) analysis of the corrosion products on stainless steel samples was performed at DELTA Beamline 8 [30]. Steel coupons were pre-conditioned and incubated in bacterial culture for one day on site. To study the surface oxide chemistry before and after incubation with bacteria, the steel coupons were measured in grazing incidence with angles below the critical angle of total reflection of the metal. Spectra were collected in the energy region of the Fe K-edge (7112.4 eV) as well as the Cr K-edge (5989.2 eV). The intensity of the monochromatic X-ray beam delivered by a double-crystal Si(111) monochromator was measured by three consecutive ionization chambers. The samples were mounted between the first and second ionization chambers. For exact energy calibration, a reference stainless steel foil was placed between the second and third chamber and measured simultaneously. The ionization chamber prior to the sample was filled with a mixture of nitrogen and helium, the chambers behind the sample and a stainless steel foil reference were filled with argon-helium mixtures adjusted to obtain an optimum absorption for each detector. The absorption spectra were collected within the range of 250 eV below to 900 eV above the K-edges with a step size of 0.3 eV in the XANES region. As references, high purity samples of relevant iron and chromium compounds were measured in transmission mode. The reference samples were provided at the beamline [31,32].

The beam spot size was adjusted to 300 µm height and 1 mm width. The samples were aligned in parallel with the beam and a rocking-scan of the tilt angle θ was performed on each sample to define the angle of grazing incidence at the exact energy for the investigated edge position. Model iron films of 80 nm thickness were investigated in an in situ cell (details described elsewhere [21]) using backscattered fluorescence detection by placing a large area PIPS (passivated implanted planar silicon) detector in immediate distance to the iron coated Kapton© window. For the measurements with model iron films, XANES spectra were collected at the start and end of the incubation experiments, without exchanging or removing the incubation media or the biofilm.

Analysis of XANES spectra was performed with the IFEFFIT program package ATHENA (Version Demeter 0.9.26, [33]). The energy-edge normalization was set to 7112.8 eV from the first inflection point. The relative K-shell contribution in the X-ray absorption spectra was calculated by fitting the pre-edge and post-edge regions in the range of -60 to -8 eV and +35 to +150 eV, respectively and adjusting the edge-jump to 1. Since the edge height is directly proportional to the amount of detected metal content, for the determination of Fe/Cr edge height ratios, non-normalized edge heights were used [34].

2.4. Electrochemical analysis and corrosion properties

All electrochemical experiments were performed in closed electrochemical cells in a three-electrode configuration. A gold wire and an Ag/AgCl/3 M NaCl electrode (C3 Prozessanalytik, Germany) were used as counter and reference electrodes, respectively. Electrochemical Impedance Spectroscopy (EIS) was used to monitor the biofilm growth for a duration of three days, the measurements were performed in the incubation medium. For the analysis of corrosion properties dynamic polarization experiments were performed after exchanging the incubation medium either with fresh minimal medium or with sea salts solution (Total Cl-content: 0.5 ± 0.06 M Sigma Aldrich, Germany). Cyclic polarization tests were performed with 1 mV/s scan rate in a potential range of -0.5 to +1.0 V vs. OCP with the current cut-off was set to 25 µA/cm^2. After the corrosion experiments, the samples were analysed by means of scanning electron microscopy with an Evo MA10 microscope (Zeiss, Germany) equipped with a SE detector operated at 7×10^{-5} mbar. After incubation experiments, the coupons were taken out of the electrochemical cell, rinsed with deionized water and cleaned in ethanol (Sigma Aldrich, 98 %) for 10 min to remove the biofilms for SEM analysis.

3. Results and discussion

3.1. Analysis of corrosion products and interface chemistry

Synchrotron based surface chemistry analysis was applied to investigate the changes in the passive film chemistry on stainless steel surfaces. The advantage of XANES is that the substrates covered with biofilms can be directly investigated after the incubation without the necessity of biofilm removal. The samples were incubated at the laboratory facilities of the DELTA Synchrotron Facility and were directly transferred to the sample stage within five minutes after removal from the culture/test media to minimize drying effects.

The first indices of changes in the surface chemistry and the effect of the presence of Fe^{3+} in the growth medium were observed in the rocking curve resulting in an angle dependent reflectivity curve (Fig. 1). In general, the analysis of the reflectivity data is an established method for the determination of thickness and interfacial roughness of layered thin film systems [35,36]. The reflectivity signal carries information on the density of the materials present in a layered film structure [37]. Considering the very thin passive film on the stainless steel surface, it is expected to acquire signals from both surface oxides/hydroxides and the underlying metallic bulk during a reflectivity scan, as well as dissolved iron diffused into the growing biofilm.

As seen in Fig. 1 a) and b), the fresh substrates before incubation present broad reflectivity peaks centred at 0.22° and 0.25°, for Fe and Cr pre-edge, respectively. During incubation with sterile or culture media the reflectivity peaks developed a shoulder at low θ-angles. This can be explained with the growth of corrosion products at the stainless steel's surface leading to a thickening of oxidic/hydroxidic surface film of lower density. With an attempt to use the information gained with the reflectivity data, Gaussian peak fitting was performed and the results are presented in Table 2 and Table 3, for the Fe and Cr pre-edge, respectively. It is clear, that usually a dedicated fit of the reflectivity data employing e.g. the Fresnel theory and the Parratt-algorithm for multilayered sample systems [38] is required, and our simplified approach does not take into account the surface and interface roughness and layer thicknesses. It is simply meant to discuss the observed double peak appearance in the reflectivity curves qualitatively, and the focus of the present work is more on the speciation of the involved Fe and Cr oxyhydroxide compounds.

The main result of the reflectivity analysis is that the ratio between the peak heights of the low θ and high θ peaks (h_{Peak2} / h_{Peak1}) increases significantly for the samples incubated in the FeCi culture indicating that a much thicker oxidic/hydroxidic surface film was formed at the biofilm-steel interface when compared to the samples incubated in the regular CN32 culture. The fitting results also indicate that the low θ peak assigned to the oxide/hydroxide film is shifted to lower angles with increasing h_{Peak2} / h_{Peak1} ratio, more pronounced with the samples incubated in the FeCi culture, which can be explained with the formation of lower density surface films, or a substantially increased roughness under these conditions. A change in the peak ratios was also observed with samples incubated in the regular CN32 culture as well as with the filtrates, however the extent of the transformation was much less pronounced. Interestingly, for all samples the Fe pre-edge reflectivity showed a higher increase in the peak ratios when compared with the Cr pre-edge reflectivity data, considering the lower energy at the Cr pre-edge, this might indicate a higher affinity of the iron grown bacteria to utilize iron and transform it into a lower density interfacial layer with higher surface roughness.

Grazing incidence XANES measurements were performed to investigate the chemistry of the surface films. To achieve a high surface sensitivity, the measurement angle was determined by computing the first derivative of the reflectivity signal and setting the measurement angle to approximately +0.01° with respect to the extremum in the first derivative, i.e. in the region of the critical angle of total reflection. The normalized XANES spectra of the samples collected at the Fe and Cr edge are presented in Fig. 2 a and b, respectively.

As a first observation, for the given angle, the signals at the Cr K-edge were much lower than at the Fe K-edge, resulting in higher noise in the data. As this effect was more pronounced with the incubated samples, it could indicate that, especially with the increasing oxide/hydroxide layer thickness and biofilm growth, Cr-containing species are located in deeper regions of the surface film. Interestingly, as seen in Fig. 2 b, in the XANES spectra of the as prepared sample before incubation a small but representative Cr(VI) signal was clearly visible as a pre-peak before the metallic edge at about 5987 eV, which disappeared after contact with the aqueous media during incubation. When comparing Fig. 2 a and b, it can be clearly seen that the majority of the changes of the oxide chemistry and growth involved iron species.

As seen in Figs. 2 a and 3 a, the samples incubated in CN32 and FeCi cultures have shown a decrease of the edge height of the metallic iron signal at 7112.4 eV, indicating the formation of an oxide film. This effect was more pronounced with the samples incubated in the FeCi culture, as already predicted from the reflectivity analysis. An isosbestic point was observed at 7128.3 eV with both incubated samples, indicating the change in the oxide chemistry with the transition between two phases only. For the CN32 culture, a slight increase of the oxidic white-line at about 7127 eV was evident, which can be attributed to the formation of Fe(III) oxides by the comparison with the reference spectra

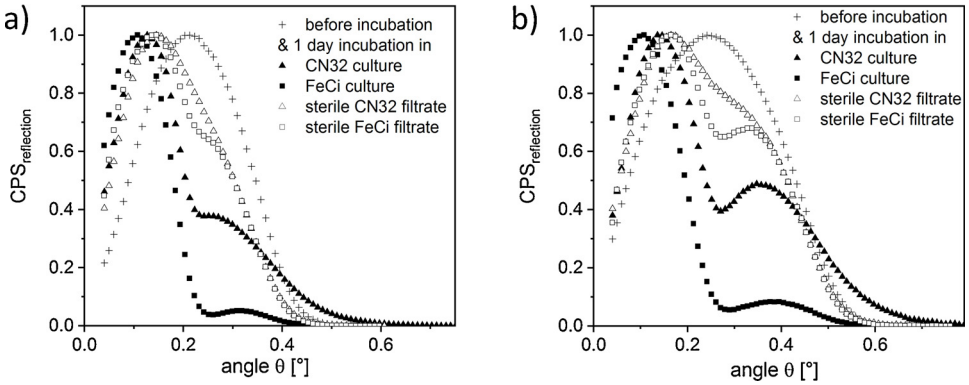

Fig. 1. Ex situ X-Ray reflectivity scans on substrates before and after incubation in culture and sterile media a) Fe pre-edge (6900 eV) and b) Cr pre-edge (5800 eV).

Table 2
Peak fitting results of the reflectivity data at Fe pre-edge (6900 eV).

Fe pre-edge	Peak #	Center [°]	FWHM	Height (h)	h_{Peak1} / h_{Peak2}
Before incubation	1	0.27	0.17	0.59	1.2
	2	0.16	0.18	0.72	
1 d incubation in sterile CN32 filtrate	1	0.27	0.16	0.49	1.9
	2	0.13	0.17	0.93	
1 d incubation in sterile FeCi filtrate	1	0.29	0.14	0.44	2.3
	2	0.13	0.18	1	
1 d incubation CN32 culture	1	0.3	0.2	0.32	3.1
	2	0.12	0.14	0.98	
1 d incubation in FeCi culture	1	0.33	0.08	0.05	20.0
	2	0.10	0.14	1	

Table 3
Peak fitting results of the reflectivity data at Cr pre-edge (5800 eV).

Cr pre-edge	Peak #	Center [°]	FWHM	Height (h)	h_{Peak2} / h_{Peak1}
Before incubation	1	0.35	0.22	0.65	1.2
	2	0.17	0.28	0.81	
1 d incubation in sterile CN32 filtrate	1	0.35	0.21	0.62	1.5
	2	0.15	0.21	0.94	
1 d incubation in sterile FeCi filtrate	1	0.36	0.19	0.61	1.6
	2	0.15	0.30	0.99	
1 d incubation CN32 culture	1	0.37	0.25	0.47	2.1
	2	0.14	0.16	0.98	
1 d incubation in FeCi culture	1	0.40	0.14	0.09	11.1
	2	0.10	0.18	1.0	

(Fig. 3a). For the samples incubated in the FeCi culture, the growth of the oxide/hydroxide film was clearly more pronounced, which also supports the large increase of the oxidic/metallic peak ratios obtained via the analysis of the reflectivity data. Since the peak positions and white lines of ferric oxides and hydroxides are very similar, a distinct identification was not possible. Nevertheless, the ex situ XANES analysis revealed the presence of an Fe(III) rich surface film.

Considering that the selected microorganism *Shewanella putrefaciens* are dissimilatory iron reducing bacteria, the presence of a ferric oxide/hydroxide rich surface film was an unexpected result. Even though the ferrous iron species could have been converted to ferric oxides at the biofilm-metal interface during incubation, it is more likely that re-oxidation takes place during the exposure to the atmosphere. Even with special care taken to minimize the time between the sample preparation and the X-ray measurements in our studies, the sample alignment, angle adjustment via reflectivity analysis and the XANES scan are completed within approximately one hour. To enable XANES measurements during incubation, an in situ measurement cell was constructed [21]. The in situ cell allows the collection of back-scattered florescence signal from thin iron film (80 nm) coated Kapton© windows without sample drying in air [21]. Model iron films were incubated with CN32 and FeCi cultures for 15 h, and at the start and the end of the experiments XANES spectra were collected via backscattered fluorescence detection for comparison to ex situ XANES results. As seen in the spectra presented in Fig. 3 b, the thin iron sample incubated in the FeCi culture developed a very strong white-line corresponding to FeO together with the nearly complete reduction of the metallic iron signal after 15 h of incubation. As reported previously [21], the sample incubated in the CN32 culture did not present any significant change in terms of surface chemistry. A small contribution of ferric oxides and hydroxides was also visible in the XANES spectra of the FeCi culture as evidenced by the presence of a shoulder peak at 7131.5 eV. With the model samples, the Fe(II) dominated signal resulted in a shift of the isosbestic point to 7121.2 eV.

The in situ XANES results clearly demonstrate that at the biofilm-metal interface, iron reducing bacteria cultivated in abundance of Fe

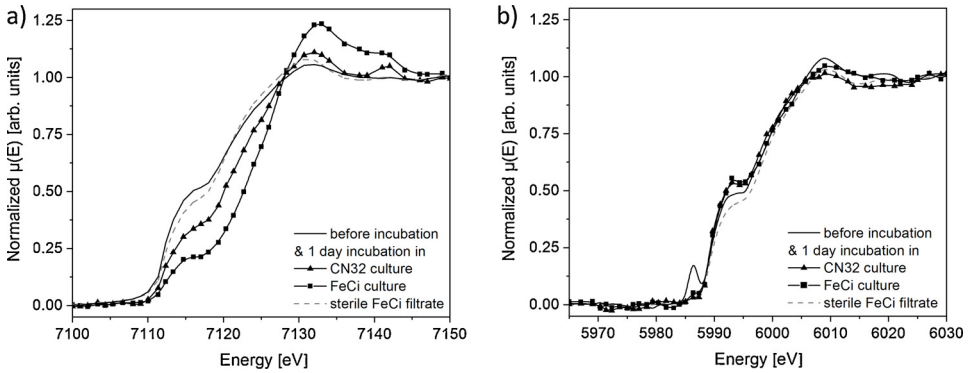

Fig. 2. Grazing incidence XANES spectra of the samples before incubation and after incubation in CN32, FeCi and sterile FeCi filtrate medium at the a) Fe K-edge, b) Cr K-edge.

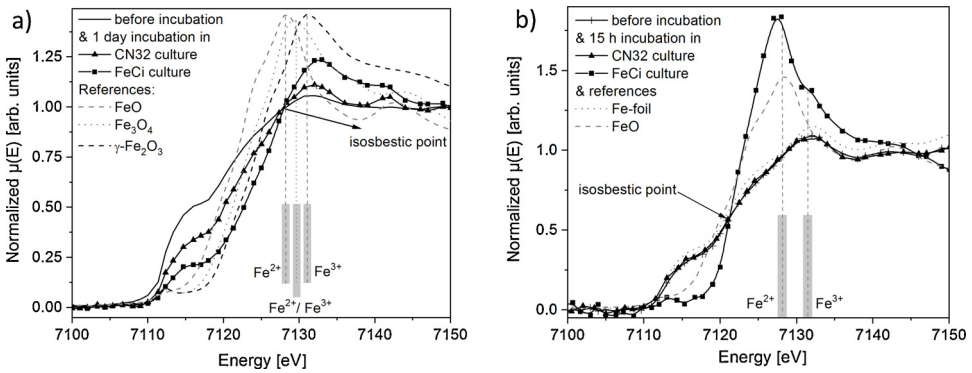

Fig. 3. Comparison of transmission XANES spectra of a) FeO, Fe_3O_4 and γ-Fe_2O_3 reference spectra with the grazing incidence XANES spectra on steel coupons and b) in situ backscattered fluorescence XANES spectra of the samples before incubation and after incubation in CN32 and FeCi culture.

(III) ions have resulted in the formation of a surface film dominated by FeO species. Even though the corrosion processes of stainless steels differ significantly from pure iron, in our opinion, it is unlikely that ferric oxides would dominate the chemistry of the surface film at the biofilm-stainless steel interface under these conditions. Therefore, we believe that the results underline, how crucial in situ techniques are for the investigation of dynamic buried interfaces under biofilms. To resolve this controversy, experiments with model Fe/Cr alloy films will be performed during the next beamtime. Nevertheless, the increase of the oxidic white-line and decrease of the metallic shoulder on pure iron in the in situ XANES results agree very well with the reflectivity data obtained on stainless steels, demonstrating that reflectivity analysis can be used as a straightforward tool to gain insights to the oxide and biofilm growth at the biofilm-metal interface.

3.2. Electrochemical corrosion analysis

Electrochemical impedance spectroscopy (EIS) was used to monitor the biofilm growth and the changes in the electrochemical properties of the passive film. As seen in the impedance spectra (Figure SI1) the majority of the changes were observed within the first day of incubation. Due to the spatial heterogeneity during early stages of biofilm formation, equivalent circuits with complex elements and a large parameter set are usually necessary to achieve an accurate description of the biofilm-metal interface. This results in a high degree of freedom in the equivalent circuit fitting process and thus the fit results tend to converge very often in local minima leading to irrational numbers for especially constant phase elements (CPEs). Therefore, the authors have opted for a qualitative analysis of impedance spectra based on the XANES analysis of the surface chemistry. The evolution of the low frequency impedance and phase shift for CN32 and FeCi samples are presented in Fig. 4.

For the CN32 culture grown in regular minimal medium without the addition of iron citrate, the low frequency impedance data is characterized by an initial decrease of impedance within the first five hours of incubation followed by a continuous increase. With the FeCi culture grown in the presence of Fe^{3+} ions a contrasting behaviour was observed, the low-frequency impedance of the system increased within the first ten hours, followed by a rapid decrease until the 15th hour of incubation. After a stagnation until the 40th hour, the impedance values started to continuously increase till the end of the experiment. The trends can be easily followed via the contour lines of respective spectra in Fig. 4 a and b. The same behaviour was also observed in the phase plots presented in Fig. 4 c and d. Between the seventh and tenth hour of incubation a phase maximum of -65° was observed with the CN32 culture, followed by a continuous decrease of the phase shift to approximately -82° during the rest of the incubation. With the FeCi culture, the phase map indicated two maxima, correlating well with the occurrence of the early and late phase impedance rises. The low frequency impedance behaviour contains information on both the formation of the biofilm and the changes in the oxide chemistry on the stainless steel surface. Both the double layer capacitance and the biofilm capacitance have an influence on the phase shift response of the system in the low frequency region. Similarly, the impedance values contain information on the charge transfer resistance of the passive film and the diffusion resistance of the biofilm.

As indicated by the XANES results and well documented in the literature [3–5], the passive film at the start of the incubation is composed of a thin mixed oxide film of iron and chromium oxy-hydroxides. For the samples incubated in FeCi culture, the initial increase of the impedance together with the secondary phase minimum centred at 0.5 Hz correlates very well with the ex situ and in situ XANES results indicating that the growing oxide film leads to an increase of the charge transfer resistance and double layer capacitance. At the later stages of biofilm formation, the pore resistance of the biofilm and the charge transfer resistance of the growing oxide film dominate the impedance response. During this transition, a decrease in the impedance and an increase of the phase shift was observed. In the case of the CN32 culture, only a minor thickening of the surface film took place, this transition in the impedance behaviour is happening with a similar trend at the beginning of the incubation.

For investigating the corrosion behaviour of incubated samples, cyclic polarization curves were measured after exchanging the culture media after incubation with sterile ShMM or sea salts solution. As seen in Fig. 5 a), no pitting was observed in the incubation media containing 15.8 mM chloride with the samples incubated with the FeCi culture. For the samples incubated in sterile culture medium, a higher passive current was observed in comparison to the samples covered with biofilm. The samples incubated in sterile control medium and CN32 culture have shown a similar pitting behaviour with pitting potentials between 0.58 mV and 0.62 mv (vs. sat. Ag/AgCl). Corrosion current (i_{corr}) values for samples incubated in CN32 and FeCi cultures calculated by fitting the Tafel region of the anodic sweep were 0.25 μA/cm^2 and 1.1 μA/cm^2, respectively. These results indicate a higher general corrosion rate for the FeCi culture.

When the electrolyte in the incubation cell was exchanged with sea salts solution containing > 0.50 M chloride, all samples have shown pitting with pitting potentials observed at 0.29 mV, 0.33 mV and 0.41 mV (vs. sat. Ag/AgCl) for samples incubated in sterile control media, CN32 culture and FeCi culture, respectively. The higher resistance to pitting observed with samples incubated in the FeCi culture correlates well with the thicker oxide film present at the biofilm-metal interface.

The representative SEM images of the samples after three days of incubation in CN32 and FeCi cultures are presented in Fig. 6 a and b, respectively. In Fig. 6 a), it can clearly be seen that the incubation alone can lead to localized corrosion on the stainless steel surface. However, on the samples incubated in FeCi culture, no pitting was observed, the

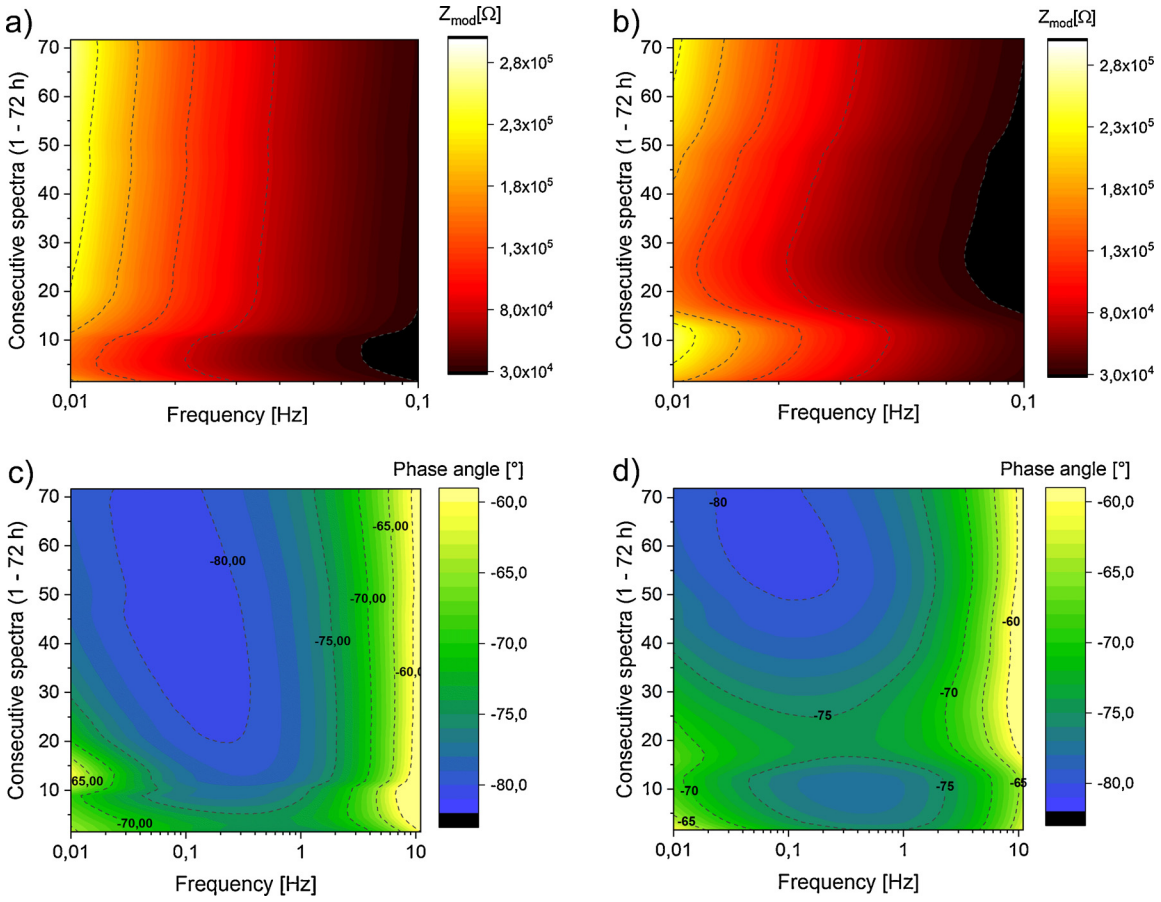

Fig. 4. Low frequency impedance (a: CN32, b: FeCi) and phase (c: CN32, d: FeCi) plots extracted from full range EIS data (Figure SI1) collected during incubation experiments.

SEM image of the severest corrosion site is presented in Fig. 6 b. In the few areas as depicted in Fig. 6 b), a preferential attack at grain boundaries was visible. As indicated by the results of the cyclic polarization studies, the FeCi biofilms have shown a protective effect.

4. Conclusions

Based on the results of the present study, the following conclusions can be drawn.

- The ex situ XANES and reflectivity analysis on stainless steel surfaces and the results of in situ XANES studies on model iron films as well as the electrochemical findings agree very well that the abundance of Fe(III) during cultivation results in an acceleration of oxide/hydroxide formation at the biofilm-iron/steel interface. The formation of a thicker oxide/hydroxide layer at the FeCi biofilm - steel interface resulted in a higher general corrosion rate but a protective effect in terms of localized corrosion. This can have a general consequence that bacteria released from active corrosion sites can show a different corrosion behaviour.
- Even though the corrosion properties of stainless steel and iron cannot be directly compared, the controversial results obtained in the surface analysis by means of ex situ and in situ XANES measurements are indications that the ex situ analysis of corrosion products, as commonly practiced, can lead to a false description of the interface chemistry, when re-oxidation processes can take place

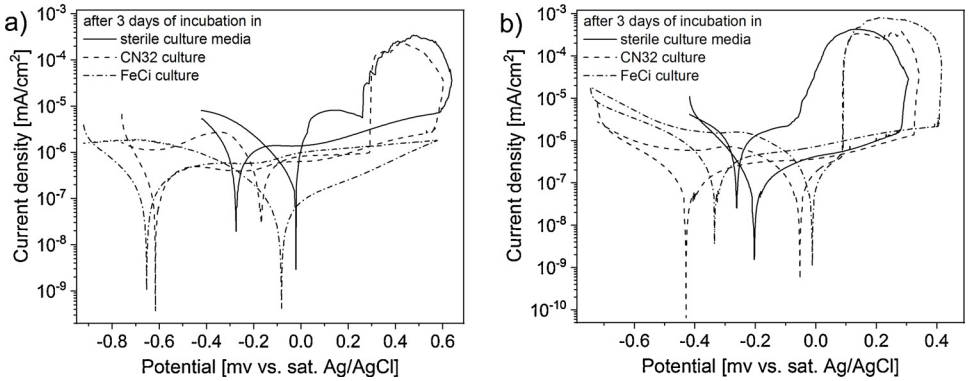

Fig. 5. Cyclic polarization curves collected after 3 days of incubation in bacterial culture (OD600 0.1) or in sterile ShMM media a) in the incubation media b) after exchanging to sea salts solution.

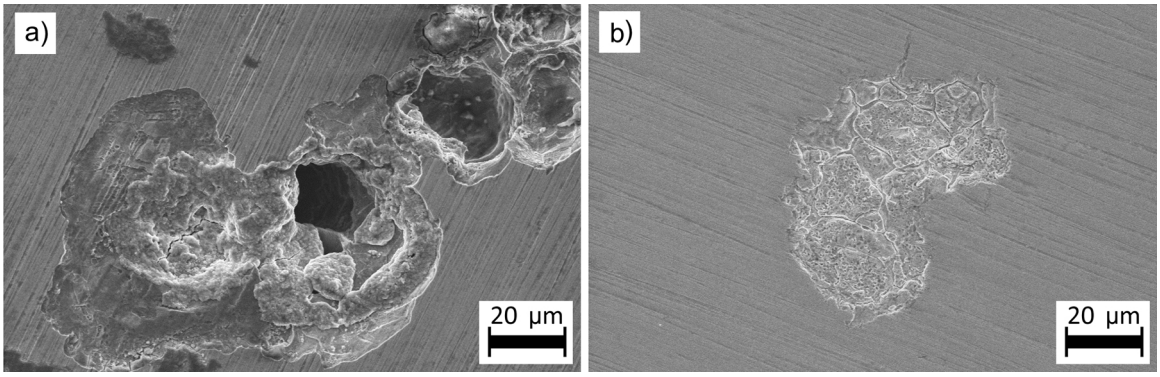

Fig. 6. SEM images of the stainless steel samples after 3 days of incubation in a) CN32 and b) FeCi culture.

in contact with the atmosphere. To take the next step in clarifying this controversy, in situ XANES experiments on FeCr13 model thin films will be performed during the next beamtime. As the passive film properties are also affected by the minute alloying elements as well as the microstructure, the model films will still be an approximation. Novel cell designs allowing in situ grazing incidence analysis on technical alloys shall enable a reliable characterization of the biofilm-metal interface.

Data availability

The raw/processed data required to reproduce these findings will be made available on request.

Funding source

This research did not receive any specific grant from funding agencies in the public, commercial, or not-for-profit sectors.

CRediT authorship contribution statement

Nina Wurzler: Formal analysis, Investigation, Methodology, Writing - original draft, Writing - review & editing. **Jan David Schutter:** Investigation, Writing - review & editing. **Ralph Wagner:** Methodology, Validation, Writing - review & editing. **Matthias Dimper:** Methodology, Writing - review & editing. **Dirk Lützenkirchen-Hecht:** Methodology, Supervision, Writing - review & editing. **Ozlem Ozcan:** Conceptualization, Supervision, Visualization, Writing - review & editing.

Declaration of Competing Interest

The authors declare that they have no known competing financial interests or personal relationships that could have appeared to influence the work reported in this paper.

Acknowledgements

Authors gratefully acknowledge the DELTA Synchrotron Facility for the assigned beamtimes and Yasser A. Shokr (Institute of Experimental Physics, Freie Universität Berlin) for technical support during iron thin film evaporation.

Appendix A. Supplementary data

Supplementary material related to this article can be found, in the online version, at doi:https://doi.org/10.1016/j.corsci.2020.108855.

References

[1] C.O.A. Olsson, D. Landolt, Passive films on stainless steels - chemistry, structure and growth, Electrochim. Acta 48 (2003) 1093–1104, https://doi.org/10.1016/S0013-4686(02)00841-1.
[2] J.J. de Damborenea, A.B. Cristóbal, M.A. Arenas, V. López, A. Conde, Selective dissolution of austenite in AISI 304 stainless steel by bacterial activity, Mater. Lett. 61 (2007) 821–823, https://doi.org/10.1016/j.matlet.2006.05.066.
[3] L. Freire, M.A. Catarino, M.I. Godinho, M.J. Ferreira, M.G.S. Ferreira, A.M.P. Simoes, M.F. Montemor, Electrochemical and analytical investigation of passive films formed on stainless steels in alkaline media, Cement Concrete Comp 34 (2012) 1075–1081, https://doi.org/10.1016/j.cemconcomp.2012.06.002.
[4] A. Seyeux, S. Zanna, A. Allion, P. Marcus, The fate of the protective oxide film on stainless steel upon early stage growth of a biofilm, Corros. Sci. 91 (2015) 352–356, https://doi.org/10.1016/j.corsci.2014.10.051.
[5] J.J. Kim, Y.M. Young, Study on the passive film of type 316 stainless steel, Int. J. Electrochem. Sci. 8 (2013) 11847–11859.
[6] A.K. Lee, D.K. Newman, Microbial iron respiration: impacts on corrosion processes, Appl. Microbiol. Biotechnol. 62 (2003) 134–139, https://doi.org/10.1007/s00253-003-1314-7.
[7] J. Philips, N. Van den Driessche, K. De Paepe, A. Prevoteau, J.A. Gralnick, J.B.A. Arends, K. Rabaey, A novel *Shewanella* isolate enhances corrosion by using metallic Iron as the Electron donor with Fumarate as the Electron acceptor, Appl. Environ. Microbiol. 84 (2018), https://doi.org/10.1128/AEM.01154-18 e01154-18.
[8] R.B. Miller 2nd, A. Sadek, A. Rodriguez, M. Iannuzzi, C. Giai, J.M. Senko, C.N. Monty, Use of an electrochemical split cell technique to evaluate the influence of *Shewanella oneidensis* activities on corrosion of carbon steel, PLoS One 11 (2016), https://doi.org/10.1371/journal.pone.0147899 e0147899.
[9] E. Marsili, D.B. Baron, I.D. Shikhare, D. Coursolle, J.A. Gralnick, D.R. Bond, *Shewanella* secretes flavins that mediate extracellular electron transfer, Proc. Natl. Acad. Sci. U. S. A. 105 (2008) 3968–3973, https://doi.org/10.1073/pnas.0710525105.
[10] J.K. Fredrickson, M.F. Romine, A.S. Beliaev, J.M. Auchtung, M.E. Driscoll, T.S. Gardner, K.H. Nealson, A.L. Osterman, G. Pinchuk, J.L. Reed, D.A. Rodionov, J.L. Rodrigues, D.A. Saffarini, M.H. Serres, A.M. Spormann, I.B. Zhulin, J.M. Tiedje, Towards environmental systems biology of *Shewanella*, Nat. Rev. Microbiol. 6 (2008) 592–603, https://doi.org/10.1038/nrmicro1947.
[11] D.R. Lovley, The microbe electric: conversion of organic matter to electricity, Curr. Opin. Biotechnol. 19 (2008) 564–571, https://doi.org/10.1016/j.copbio.2008.10.005.
[12] A.A. Carmona-Martinez, F. Harnisch, U. Kuhlicke, T.R. Neu, U. Schroder, Electron transfer and biofilm formation of *Shewanella putrefaciens* as function of anode potential, Bioelectrochemistry 93 (2013) 23–29, https://doi.org/10.1016/j.bioelechem.2012.05.002.
[13] N. Kip, J.A. van Veen, The dual role of microbes in corrosion, ISME J. 9 (2015) 542–551, https://doi.org/10.1038/ismej.2014.169.
[14] L.K. Herrera, H.A. Videla, Role of iron-reducing bacteria in corrosion and protection of carbon steel, Int. Biodeter. Biodegr. 63 (2009) 891–895, https://doi.org/10.1016/j.ibiod.2009.06.003.
[15] H.A. Videla, L.K. Herrera, Microbiologically influenced corrosion: looking to the future, Int. Microbiol. 8 (2005) 169–180.
[16] M. Dubiel, C.H. Hsu, C.C. Chien, F. Mansfeld, D.K. Newman, Microbial iron respiration can protect steel from corrosion, Appl. Environ. Microbiol. 68 (2002) 1440–1445, https://doi.org/10.1128/aem.68.3.1440-1445.2002.
[17] J. Monnier, S. Réguer, E. Foy, D. Testemale, F. Mirambet, M. Saheb, P. Dillmann, I. Guillot, XAS and XRD in situ characterisation of reduction and reoxidation processes of iron corrosion products involved in atmospheric corrosion, Corros. Sci. 78 (2014) 293–303, https://doi.org/10.1016/j.corsci.2013.10.012.
[18] P. Schmuki, M. Buchler, S. Virtanen, H.S. Isaacs, M.P. Ryan, H. Bohni, Passivity of iron in alkaline solutions studied by in situ XANES and a laser reflection technique, J. Electrochem. Soc. 146 (1999) 2097–2102, https://doi.org/10.1149/1.1391897.
[19] M. Kerkar, J. Robinson, A.J. Forty, Insitu structural studies of the passive film on Iron and Iron chromium-Alloys using X-Ray absorption-spectroscopy, Faraday

Discuss. 89 (1990) 31–40, https://doi.org/10.1039/dc9908900031.
[20] A.J. Davenport, M. Sansone, High-resolution in-situ xanes investigation of the nature of the passive film on Iron in a ph 8.4 borate buffer, J. Electrochem. Soc. 142 (1995) 725–730, https://doi.org/10.1149/1.2048525.
[21] N. Wurzler, J.D. Schutter, R. Wagner, M. Dimper, D. Lützenkirchen-Hecht, O. Ozcan, Trained to corrode: cultivation in the presence of Fe(III) increases the electrochemical activity of iron reducing bacteria - an in situ electrochemical XANES study, Electrochem. commun. (2020) 106673, https://doi.org/10.1016/j.elecom.2020.106673.
[22] S. Virtanen, P. Schmuki, A.J. Davenport, C.M. Vitus, Dissolution of thin iron oxide films used as models for iron passive films studied by in situ x-ray absorption near-edge spectroscopy, J. Electrochem. Soc. 144 (1997) 198–204, https://doi.org/10.1149/1.1837385.
[23] A.J. Davenport, A.J. Dent, M. Monir, J.A. Hammons, S.M. Ghahari, P.D. Quinn, T. Rayment, XANES study of the chemistry of molybdenum in artificial corrosion pits in 316L stainless steel, J. Electrochem. Soc. 158 (2011) C111–C117, https://doi.org/10.1149/1.3559457.
[24] H.S. Isaacs, P. Schmuki, S. Virtanen, In situ studies of corrosion using X-ray absorption near spectroscopy (xanes), in: D.C. Baer, C.R. Davis, G.D. Halada (Eds.), Electrochemical Society Series, 2001, pp. 271–281.
[25] B.C. Barlow, A. Situm, B. Guo, X.X. Guo, A.P. Grosvenor, I.J. Burgess, X-ray microprobe characterization of corrosion at the buried polymer-steel interface, Corros. Sci. 144 (2018) 198–206, https://doi.org/10.1016/j.corsci.2018.08.051.
[26] A. Situm, X.X. Guo, B. Guo, B.C. Barlow, I.J. Burgess, A.P. Grosvenor, A spectromicroscopy study of the corrosion of fusion-bonded epoxy-coated rebar, Surf. Interface Anal. 51 (2019) 525–530, https://doi.org/10.1002/sia.6613.
[27] T.P. Trainor, A.S. Templeton, P.J. Eng, Structure and reactivity of environmental interfaces: application of grazing angle X-ray spectroscopy and long-period X-ray standing waves, J. Electron Spectros. Relat. Phenomena 150 (2006) 66–85, https://doi.org/10.1016/j.elspec.2005.04.011.
[28] T.R. Garrett, M. Bhakoo, Z.B. Zhang, Bacterial adhesion and biofilms on surfaces, Prog. Nat. Sci. 18 (2008) 1049–1056, https://doi.org/10.1016/j.pnsc.2008.04.001.
[29] J. Miller, K. Lee, Experiments in molecular genetics, Cold Spring Harbor Laboratory, Cold Spring Harbor, NY, 1972.
[30] D. Lützenkirchen-Hecht, R. Wagner, U. Haake, A. Watenphul, R. Frahm, The materials science X-ray beamline BL8 at the DELTA storage ring, J. Synchrotron Rad. 16 (2009) 264–272, https://doi.org/10.1107/S0909049509000508.
[31] D. Lützenkirchen-Hecht, L. Müller, L. Hoffmann, R. Wagner, Analysis of engine motor oils by X-ray absorption and X-ray fluorescence spectroscopies, X-ray Spectrom. 43 (2014) 221–227, https://doi.org/10.1002/xrs.2543.
[32] D. Lützenkirchen-Hecht, D. Wulff, R. Wagner, R. Frahm, U. Holländer, H.J. Maier, Thermal anti-oxidation treatment of CrNi-steels as studied by EXAFS in reflection mode: the influence of monosilane additions in the gas atmosphere of a continuous annealing furnace, J. Mater. Sci. 49 (2014) 5454–5461, https://doi.org/10.1007/s10853-014-8257-5.
[33] B. Ravel, M. Newville, ATHENA, ARTEMIS, HEPHAESTUS: data analysis for X-ray absorption spectroscopy using IFEFFIT, J. Synchrotron Radiat. 12 (2005) 537–541, https://doi.org/10.1107/S0909049505012719.
[34] L.J. Oblonsky, M.P. Ryan, H.S. Isaacs, In situ XANES study of the formation and reduction of the passive film formed on Fe in acetate solution, Corros. Sci. 42 (2000) 229–241, https://doi.org/10.1016/S0010-938x(99)00078-5.
[35] D. Lützenkirchen-Hecht, M. Wagemaker, P. Keil, A.A. van Well, R. Frahm, Ex situ reflection mode EXAFS at the Ti K-edge of lithium intercalated TiO2 rutile, Surf. Sci. 538 (2003) 10–22, https://doi.org/10.1016/S0039-6028(03)00722-2.
[36] J. Just, D. Lutzenkirchen-Hecht, O. Muller, R. Frahm, T. Unold, Depth distribution of secondary phases in kesterite Cu_2ZnSnS_4 by angle-resolved X-ray absorption spectroscopy, APL Mater. 5 (2017), https://doi.org/10.1063/1.5000306 126106-126101-126107.
[37] C.A. Helm, H. Mohwald, K. Kjaer, J. Alsnielsen, Phospholipid monolayer density distribution perpendicular to the water-surface - a synchrotron X-Ray reflectivity study, Europhys. Lett. 4 (1987) 697–703, https://doi.org/10.1209/0295-5075/4/6/010.
[38] L.G. Parratt, Surface studies of solids by total refiection of X-Rays, Phys. Rev. 95 (1954) 359–369, https://doi.org/10.1103/PhysRev.95.359.